Further Results on the Sensitivity of Simulated Storm Precipitation Efficiency to Environmental Temperature

CHARLES COHEN AND EUGENE W. MCCAUL JR.

Universities Space Research Association, Huntsville, Alabama

(Manuscript received 24 May 2006, in final form 24 August 2006)

ABSTRACT

A method is devised for diagnosing the condensation rate in simulations using the Regional Atmospheric Modeling System (RAMS) model, where ice-liquid water potential temperature is a prognostic variable and an iterative procedure must be used to diagnose the temperature and water vapor mixing ratio from ice-liquid water potential temperature. The condensation rate is then used to compute the microphysical precipitation efficiency (PE), which is defined as the ratio of the precipitation rate at the ground to the sum of the condensation and deposition rates. Precipitation efficiency is compared for pairs of numerical simulations, initialized with soundings having all key environmental parameters identical except for their temperature. The authors' previous study showed that with a colder initial sounding, the conversion of cloud water to precipitation is relatively inefficient, but updrafts are stronger and there is relatively less evaporation of precipitation, with the net result being a larger climatological PE in the colder environment. Here, the authors consider the time lag between condensation and precipitation and demonstrate that in calculating a properly lagged microphysical PE, the combined effect of the decreased production of precipitation and the decreased evaporation is that the temperature of the initial soundings has no significant influence on the microphysical PE. To the authors' knowledge, this is the first time that the lag has been used to compute PE. These results concerning PE are relevant only to deep convection.

1. Introduction

In the Regional Atmospheric Modeling System, version 3b (RAMS; Pielke et al. 1992; Walko et al. 1995), ice-liquid water potential temperature, θ_{il}, is a prognostic variable and an iterative procedure is used to diagnose temperature T and water vapor mixing ratio q_v from θ_{il}. The following semiempirical formula is used in the model:

$$\theta = \theta_{il}\left[1 + \frac{L_{lv}(T_0)q_l}{C_p \max(T, 253)} + \frac{L_{iv}(T_0)q_i}{C_p \max(T, 253)}\right], \quad (1)$$

where θ is potential temperature, L_{lv} and L_{iv} are the latent heats of vaporization and sublimation, respectively, $T_0 = 273.16$, the triple point for water, q_l and q_i are the mixing ratios of liquid water and of ice, respectively, and C_p is the specific heat of dry air at constant pressure.

There are advantages, explained by Tripoli and Cotton (1981), to using θ_{il} as a prognostic variable in simulations of deep convection. It eliminates the need for a saturation adjustment; it reduces the number of time-dependent variables by one; and temperature tendencies due to phase changes of water need not be considered explicitly. However, there is a potentially serious disadvantage to using θ_{il} in a research model. It is difficult for a researcher to compute a water budget or a heat budget because there is no place in the model code where the rate of condensation of water vapor to cloud water or the rate of evaporation of cloud water is computed.

Precipitation efficiency (PE), which is an important part of a water budget, has been used to study, for example, orographic rain (Browning et al. 1975), hailstorms (Knight and Knight 2001), flash floods (Doswell et al. 1996), hydroclimatology (Mohamed et al. 2005a,b), climate change (Lindzen et al. 2001), weather modification (Hudak and List 1988), and upper-

Corresponding author address: Charles Cohen, Universities Space Research Association, 320 Sparkman Drive, Huntsville, AL 35805.
E-mail: cohen@usra.edu

DOI: 10.1175/MWR3380.1

tropospheric aerosols (Cui and Carslaw 2006). The wide range of applications of PE derives in part from its many different definitions, which can be a source of confusion.

Diagnosing a condensation rate may be necessary in order to compute PE, depending on how this quantity is defined. McCaul et al. (2005) distinguished the climatological precipitation efficiency (CPE) from the microphysical precipitation efficiency (MPE). They computed only the former, which is the ratio of the precipitation at the ground to the precipitable water. Because the model uses θ_{il} as a prognostic variable, they provided speculative comments but did not compute numerical values for the MPE, which we define in our numerical modeling study as the ratio of the precipitation rate at the ground to the total condensation plus deposition rates. In observational studies, where the condensation and deposition rates cannot be directly measured or computed, MPE is often defined as the ratio of the precipitation at the ground to the water vapor inflow, either through cloud base (Fankhauser 1988) or through the boundary of the volume containing the storm (Doswell et al. 1996). The intent of this latter definition is that the volume is a relatively small one that just surrounds the storm. In contrast, Schär et al. (1999) divided the precipitation rate by the sum of the evapotranspiration and the water vapor influx into the domain, where the domain was much larger than an individual storm. Without the evapotranspiration, this definition is somewhat similar to that of Raddatz (2005) and Mohamed et al. (2005a,b), who defined PE as the fraction of the area-average horizontal water vapor flux that falls as rain. In an observational study, Cotton et al. (1989) defined PE as the ratio of the precipitation at the ground to the water vapor made available to the storm, where the latter was defined as the sum of the rates of horizontal convergence and horizontal advection of water vapor and the rates of surface evaporation and evaporation of condensate. In what may be a hybrid of CPE and MPE, Brooks and Wilhelmson (1992) defined a PE in their numerical simulations as the ratio of precipitation at the ground to the sum of the water vapor in the initial state plus the net amount transported through the lateral boundaries. Rauber et al. (1996) computed the efficiency of trade wind clouds in returning water vapor evaporated from the ocean surface back to the ocean through precipitation, thus defining PE as the ratio of the precipitation rate to the surface moisture flux. Lau and Wu (2003) defined the efficiency of production of precipitation as the reciprocal of an autoconversion time scale, leaving any subsequent evaporation of precipitation out of the definition.

As in the present study, Weisman and Klemp (1982) computed PE in 2-h-long numerical simulations. They noted that PE would probably be higher if computed over the storm's entire life, due to continuing rainout and little new condensation during the dissipation phase. For the five simulations shown in Table 2 of Ferrier et al. (1996), the mass of suspended condensate at the end of the simulations ranges from 19% to 44% of the rainfall at the ground, but this was not accounted for in computing PE. In his observational study, Fankhauser (1988) recognized this type of problem but did not propose a solution, except to say that a significant and representative portion of a storm's history should be included in deriving fluxes. In the present study, we use the time lag between condensation and precipitation fallout in our calculation of PE, enabling us to account for the limited duration of the simulations. To our knowledge, this has not been done before.

McCaul et al. (2005) investigated the physical processes that influence the MPE in numerically simulated storms, though they did not attempt to assess it quantitatively. Here, we show how this quantity can be computed in a model that uses θ_{il} as a prognostic variable, accounting for the open lateral boundaries and the limited duration of the simulation. We include in our calculations only the second hour of the 2-h simulations in order to avoid the somewhat artificial effect of the initial warm bubble.

In a numerical modeling study, Ferrier et al. (1996) showed that PE depends on the tilt of the updrafts (controlled largely by the ambient wind shear) and on the relative humidity of the large-scale environment. With six of the idealized initial soundings employed here, as explained in section 2, wind shear does not vary nor does the environmental relative humidity above cloud base. Unlike what happens with CPE, we show that, for long-lasting storms in a moist environment, MPE does not vary with the environmental temperature when the time lag between condensation and precipitation fallout is considered. We also briefly examine the influence of environmental relative humidity on MPE.

2. Method

We use RAMS version 3b with modifications and improvements described in McCaul and Cohen (2002) and McCaul et al. (2005). The model domain is 75 km on each side and 24.5 km deep, with a horizontal grid interval of 500 m and a vertical grid interval that ranges from 250 m at the surface to 750 m at 20-km altitude.

We examine the results of 10 simulations that are part of an eight-dimensional parameter space study derived from McCaul and Weisman (2001) and McCaul

and Cohen (2002) and described in detail in McCaul et al. (2005). All of the simulations are initialized with idealized soundings, which are labeled using the nomenclature explained in Table 1 of McCaul et al. (2005). Here, we have first selected six soundings, all with a semicircular hodograph with a radius of 12 m s^{-1}, with the buoyancy and wind shear concentrated in the lower troposphere, with LCL and LFC height of 1.6 km, and with a free-troposphere relative humidity (FTRH) of 90% everywhere above the LCL. The soundings vary by the three different values of CAPE and two different values of LCL temperature, and by implication, precipitable water. Because these are the only variables in the six 90% FTRH soundings used here, we abbreviate the experiment names used in McCaul et al. (2005) by specifying e1, e2, or e3 for the CAPE of either 800, 2000, or 3200 J kg^{-1}, respectively, and p3 or p6 for the precipitable water of 30 or 60 mm, respectively, along with h9 for 90% FTRH. In addition, we examine simulations with a CAPE of 2000 J kg^{-1} and an FTRH of either 80% or 70% above the LCL, labeled with h8 or h7.

As discussed in McCaul et al. (2005), convection is initiated with circularly symmetric warm and moist bubbles placed near the center of the domain. The amplitude of the bubbles varies among the h9 simulations in order to ensure that the equivalent potential temperature perturbations are similar across pairs of p3 and p6 experiments. We also find it necessary to increase the strength of the warm bubbles slightly for the h8 and h7 simulations in order to produce sustained deep convection (McCaul and Cohen 2004).

To compute the rates of condensation and evaporation, we have redone the simulations of interest, with the value of q_v being assigned to a passive tracer at the beginning of each time step. This passive tracer is forecast using only those processes that might change q_v without allowing any change of phase of water. Specifically, the tracer evolves only by diffusion and advection, while at the same time the actual q_v is forecast by diffusion, advection, and microphysical processes. The saturation mixing ratio is affected by the change in temperature that is diagnosed from the forecast θ_{il} and by the forecast pressure. At the end of the time step, q_v is diagnosed and the amount of condensation or evaporation is computed from the difference between q_v and the mixing ratio of the passive tracer, multiplied by the mass of dry air in the grid box.

When a negative value of any one of the different prognostic water species is set to zero in RAMS, this increase in water substance is balanced by a proportionate decrease in other species at the same grid point. Although no latent heat release is intended by this, it is obvious from (1) that a change in either liquid or frozen condensate mixing ratio will influence the temperature that is diagnosed from θ_{il}. Therefore, we treat the process of setting negative values to zero as a phase change and do not apply any adjustment to q_v from this procedure to the passive tracer.

Because this method of diagnosing condensation or evaporation does not distinguish between liquid and frozen condensate, the results can be used in a water budget but not to compute latent heat release. For convenience in discussing the water budget, we therefore use "condensation" to refer to condensation and deposition and "evaporation" to refer to evaporation and sublimation. Another limitation is that if liquid water evaporates and water vapor is deposited onto ice at the same grid point in the same time step, only the net amount of evaporation or condensation would be detected by this method.

We also compute the flux of condensate that exits the domain through the lateral boundaries, and because we are interested only in the second hour of each simulation, we account for the change in the condensate that exists in the atmosphere during that hour.

3. Results

a. Condensate budget

Table 1 shows the water budget for the six h9 simulations, with all quantities computed for the second hour, in 10^8 kg. The condensation (C) should be equal to the sum of the evaporation (E), the precipitation at the ground (R), the net flux of condensate exiting the domain through the lateral boundaries (B), and the change over time in suspended condensate in the domain (S):

$$C = E + R + B + S. \tag{2}$$

This equation is similar to Eq. (1) of Ferrier et al. (1996), except that they assumed, as Shepherd et al. (2001) point out, no flux through the lateral boundaries. The error, which is shown in the table, is the sum of the four quantities on the right side of (2) minus the condensation. For all six simulations it is negative, ranging from 2.1% to 3.8% of the amount of condensation.

The consistent imbalance in the water budget is unavoidable because RAMS does not conserve mass (Tripoli and Cotton 1982, their section 3d). For example, the diabatic contribution to the pressure equation is ignored in RAMS, as explained by Bryan and Fritsch (2002) and Medvigy et al. (2005). To estimate the effect of this term on the condensate budget, we compute

TABLE 1. Condensate budget, using the symbols in (2), for simulations with initial humidity of 90% above the LCL. All numbers are in 10^8 kg during the second hour. Numbers may not add exactly due to rounding.

	e1p3h9	e1p6h9	e2p3h9	e2p6h9	e3p3h9	e3p6h9
C	167	180	306	489	336	413
E	52	77	73	158	75	132
R	86	73	141	220	133	146
B	17	2	37	23	52	18
S	9	24	44	71	64	102
Error $= E + R + B + S - C$	−4	−4	−9	−15	−12	−16
Loss of condensate due to absence of diabatic contribution to the pressure equation	−4	−4	−11	−20	−12	−19
Part of change in suspended condensate that is rain + hail + graupel	50%	68%	51%	59%	43%	67%

what the change in pressure would have been if this term had been included in the pressure equation in RAMS, using equation set B in Table 1 of Bryan and Fritsch (2002). We then apply the ideal gas law to convert this change in pressure to a change in dry-air density, and finally, for each grid box, we multiply the change in dry-air density by the condensate mixing ratio and by the volume of the grid box. The result is an estimate of the loss of condensate due to condensational heating or the gain of condensate due to evaporational cooling. The net loss of condensate from this term in the model domain during the second hour, shown in Table 1, is roughly the same size as the error in the condensate budget.

To compute the precipitation efficiency in a simulation that is limited in both horizontal area and duration, it can be misleading to simply divide the precipitation by the condensation. Notice, for example, that for the e1 and e3 cases, the increase over time in suspended condensate is a much larger fraction of the precipitation at the ground for the p6 cases. Furthermore, for the p6 cases a larger fraction of this additional suspended condensate is composed of rain, graupel, and hail while for the p3 cases more of it is made up of the relatively slowly precipitating ice species (Table 1). As shown in McCaul et al. (2005), the p3 cases apparently convert condensate to precipitation less efficiently and have larger or denser cirrus anvils. Thus, it appears that if the simulations had been run for a longer time, the precipitation efficiency would have increased more for the p6 cases. This can be accounted for by considering the time lag between condensation and precipitation fallout, as shown below in section 3b.

Notice also that the flux of condensate through the lateral boundaries is a much larger fraction of the precipitation at the ground for the p3 cases. As shown by McCaul et al. (2005), the p3 storms are stronger, with more updraft mass flux, especially in the upper troposphere. However, because the flux of condensate through the boundaries is almost entirely in the cirrus anvil (Fig. 1), if the domain had been much larger this, condensate would most likely not have reached the ground as precipitation anyway. This conclusion is supported by Ferrier et al. (1996, their Table 6), who found that when PE was defined as the ratio of precipitation at the ground to condensation, as long as it was calculated from a region at least 50 km wide that includes the convection, it did not vary much with the size of the region.

b. *Precipitation efficiency*

When we average, over the second hour, the precipitation and condensation rates shown as time series in Fig. 2, and then compute the ratios, we obtain the average PE for each simulation, shown to the right of its name in each panel of the figure. The values range from 0.35 to 0.51 and are larger with the colder p3 soundings. However, it takes some time after vapor condenses before the precipitation forms and finally reaches the ground. In their numerical simulations, Shepherd et al. (2001) noted a lag of roughly 8–10 min between condensation and precipitation. Fankhauser (1988) found that peaks in rainout lag water vapor inflow maxima by periods of 20–40 min. Similarly, Frank and Cohen (1987), using the data of Cooper et al. (1982), derived a lag of 20 min between updraft and downdraft mass fluxes in convective clouds. The need to account for the time lag between condensation and precipitation fallout in computing PE can be inferred from the calculation by Auer and Marwitz (1968) of a PE of 120% for a storm in Colorado.

In our simulations, notice that for e1p3h9 there is a local minimum in the condensation rate just before 78 min (Fig. 2) and a local minimum in the precipitation rate just before 100 min. For e3p6h9, the slope of the time series of condensation rate increases at 102 min,

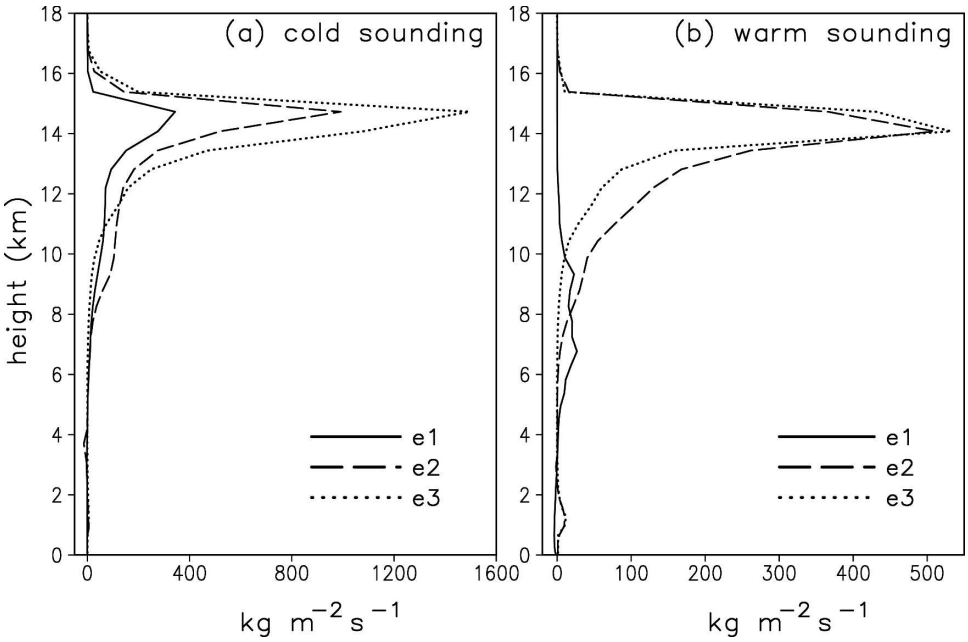

FIG. 1. Flux of condensate through the lateral boundaries (kg m^{-2} s^{-1}) during the second hour for (a) e1p3h9 (solid), e2p3h9 (dashed), and e3p3h9 (dots) and (b) e1p6h9 (solid), e2p6h9 (dashed), and e3p6h9 (dots).

with no corresponding increase in the slope of the time series of precipitation rate before the simulation ends 18 min later. For some of the simulations, the only clear evidence of a lag is the time between the initial condensation and the first arrival of precipitation at the ground, which is roughly 20 min for all of the h9 simulations. We are thus prompted to consider a reanalysis of the PE by dividing the precipitation by the condensation that occurred 20 min earlier.

Before we use this lag to revise our calculations of PE, we need to understand the change in the clouds over time. For each of the six simulations, Fig. 3 shows the time series of the horizontal updraft area in the model domain at each level, and Fig. 4 shows time series of the maximum vertical velocity at each level during each 5-min interval. The simulations are not all similar. For e1p6h9, the rapid increase in the condensation during the second hour is due to the strengthening and increase in depth of the updraft (Fig. 4), not to any increase in horizontal area in the lower or middle troposphere (Fig. 3). The opposite is true for e3p3h9, which shows an increase in updraft area, especially at around 5–10-km altitude, without any increase in maximum upward velocity. In e3p6h9, the initiation of updrafts at the gust front, which appears as an increase in updraft area in Fig. 3, causes a rapid increase in condensation after 102 min, but at the close of the simulation these clouds have not yet grown tall or strong. The two e2 simulations are generally similar, with the larger rate of increase over time in the condensation rate for e2p6h9 due to the larger precipitable water.

To examine the effect of the lag between condensation and precipitation in our simulations, we tentatively estimate the lag to be 20 min for all simulations. (This estimate is examined below in section 3d.) Figure 5 shows the time series of precipitation rate for 20 to 120 min (the solid curves), compared to the condensation rate for 0 to 100 min multiplied by the average precipitation efficiency for the second hour (i.e., multiplied by the numbers shown in Fig. 2; the dashed curves). Except for the e1p3h9 simulation, the solid curves in Fig. 5 are above the dashed curves, indicating that the PE is really larger than the quantities obtained from dividing the time-averaged precipitation by the simultaneous time-averaged condensation. We are therefore motivated to consider a PE that, when multiplied by the condensation rate for 40 to 100 min, provides the best fit to the precipitation rate for 60 to 120 min. This is obtained by minimizing the mean squared difference. The results, shown at the lower right of each panel of Fig. 5, when multiplied by the condensation rates, produce the dotted curves in that figure. Independent of any details of the time series, the precipitation efficiency that accounts for the lag is higher than our first calculation simply because the precipitation and condensation rates are both increasing with time. Using the

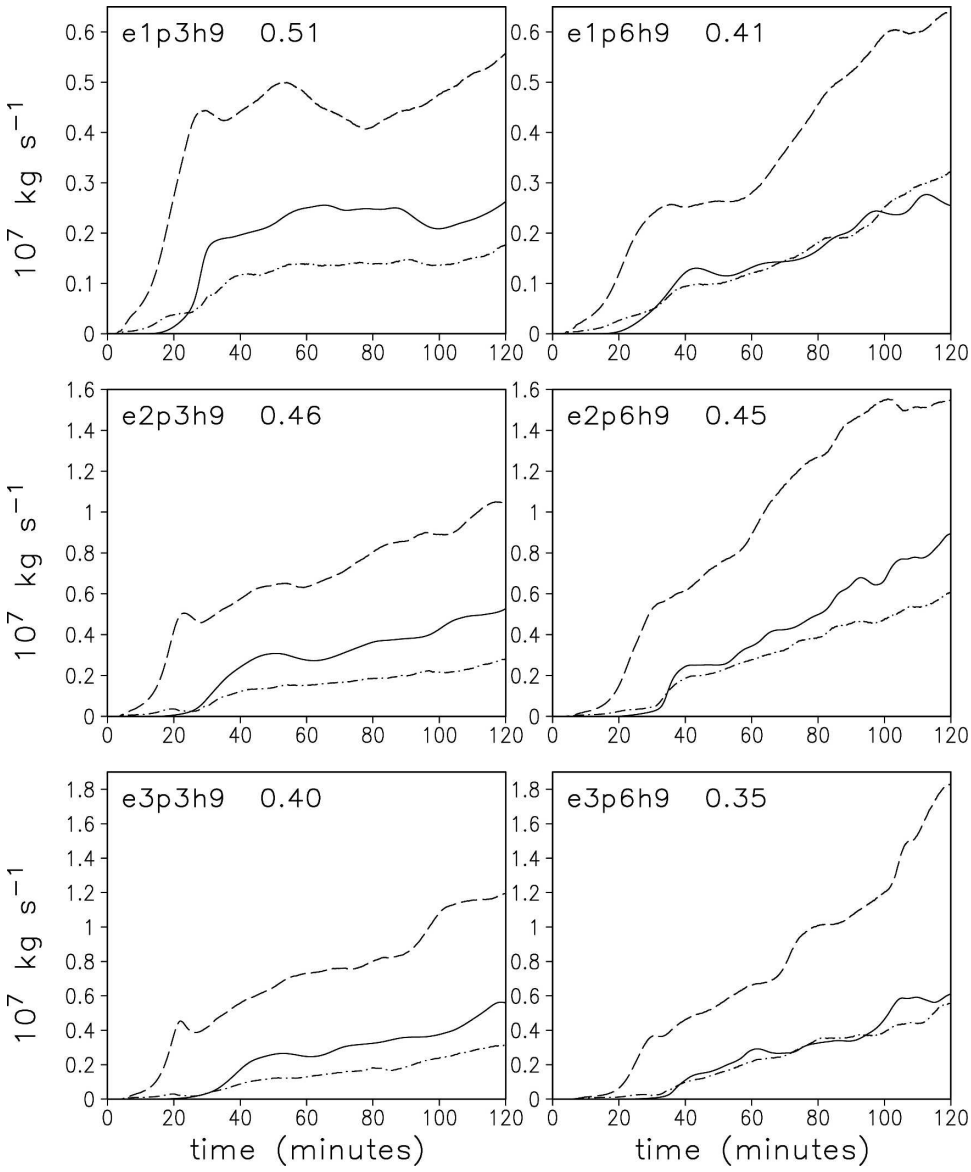

FIG. 2. Time series of rates of precipitation (solid), condensation (dashed), and evaporation (dot–dashed) in the whole domain (10^7 kg s^{-1}). The average precipitation efficiency during the second hour for each simulation is shown to the right of its name.

earlier condensation rate, which is smaller, produces a larger PE.

c. Simulations with lower initial RH

It is well known that PE is smaller for storms that develop in environments with lower FTRH (e.g., Ferrier et al. 1996; Lucas et al. 2000; Shepherd et al. 2001). Table 2 shows the condensate budget for the h7 and h8 experiments, and Fig. 6 includes time series of their condensation and precipitation. In contrast to the h9 simulations, the suspended condensate decreases during the second hour (Table 2), indicating dissipating convection. The average PE for each simulation, shown to the right of its name in each panel of Fig. 6, is computed by averaging the simultaneous precipitation and condensation rates over the second hour and then computing the ratios. The PE of 0.9 for e2p3h7 is obviously characteristic of the decaying stage of convection. From Fig. 6 we do not see any clear trends in PE as a function of FTRH. However, when we compute PE using a lag of 20 min, as above, we see (Fig. 7) that the PE does in fact decrease with decreasing midtropospheric relative humidity, as expected.

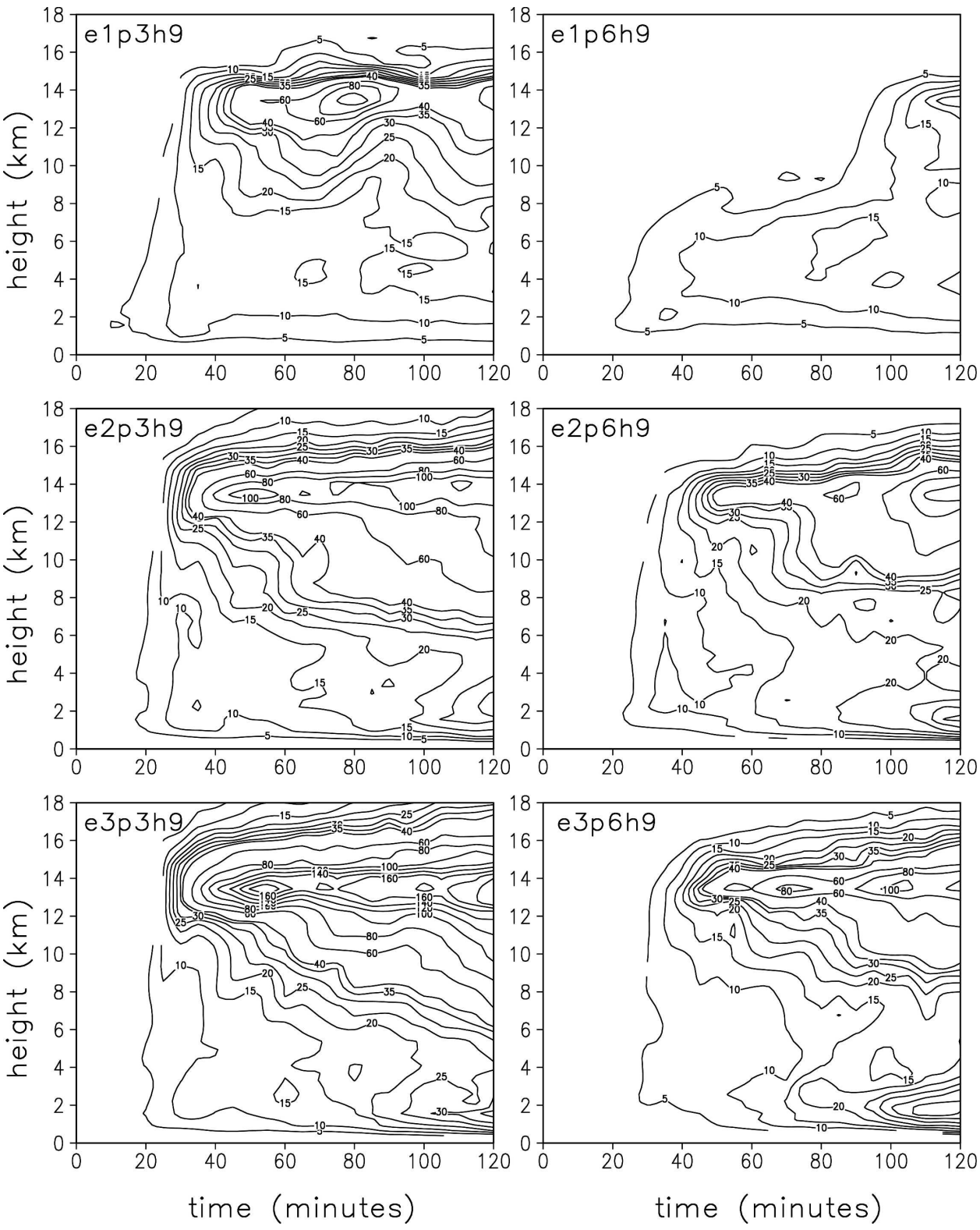

FIG. 3. Time series of horizontal updraft area in the model domain in units of 10^7 m^2. Data are from instantaneous model output every 5 min. Contour intervals are 5 units up to 40 and 20 above 40.

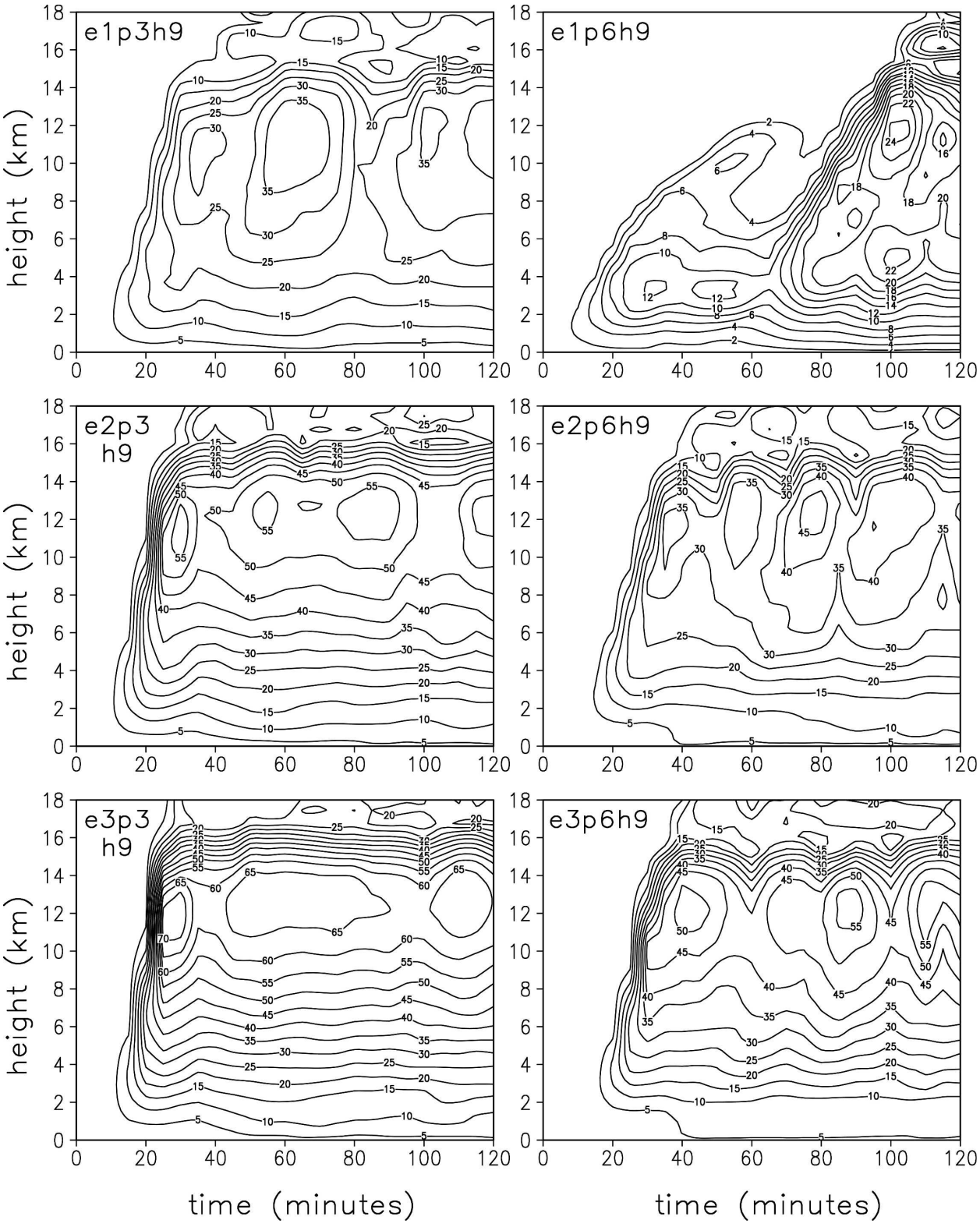

FIG. 4. Time series of maximum w (m s^{-1}) in the model domain. Data are from model output every 5 min and show the maximum w during the previous 5 min.

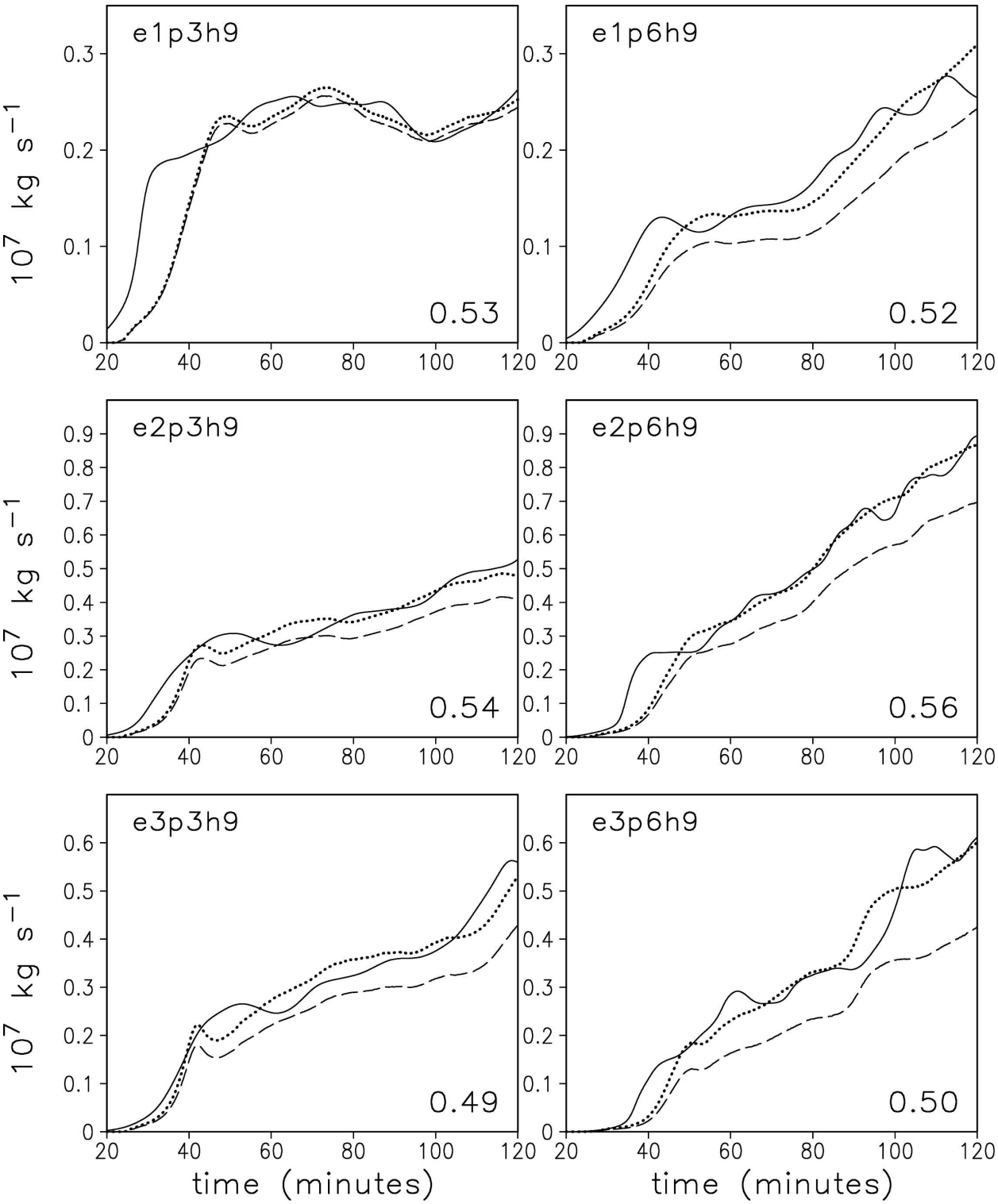

FIG. 5. Time series of the precipitation rate for 20 to 120 min (solid) and the condensation rate for 0 to 100 min multiplied by the precipitation efficiency for the second hour (dashed) in the whole domain (10^7 kg s^{-1}). The dotted curves are the condensation rates multiplied by the constant (shown in the lower-right corner of each panel) that provides the best fit to the precipitation rate during the second hour. The times on the horizontal axes apply only to the precipitation; the condensation is 20 min earlier.

TABLE 2. Condensate budget, using the symbols in (2), for simulations with initial relative humidity less than 90%. All numbers are in 10^8 kg during the second hour. Numbers may not add exactly due to rounding.

	e2p3h7	e2p3h8	e2p6h7	e2p6h8
C	21	110	30	151
E	16	40	30	69
R	19	58	15	68
B	13	20	7	12
S	−27	−12	−22	−2
Error = $E + R + B + S - C$	−0.4	−3.0	−0.4	−3.7
Loss of condensate due to absence of diabatic contribution to the pressure equation	−0.5	−3.4	−0.4	−4.8

In contrast to the h9 simulations, for which using the earlier condensation rate produces a lagged PE that is larger than the original, here the lagged PE is smaller than the original because the precipitation and condensation rates are both decreasing with time. The decrease in PE computed with the lag is greater for the h7 simulations, in which the convection weakens more rapidly over time.

Note that for the p6 cases shown in Fig. 7, with a 20-min lag the precipitation peaks at around 40 min precede the condensation peaks, indicating that the 20-min lag may be excessive. However, as shown in Fig. 8, which is examined in the next subsection, no matter how we decrease the lags for e2p6h7 and e2p6h8, the PE still decreases with FTRH.

d. Lag between condensation and precipitation

For each pair of h9 simulations, the lagged PE (Fig. 5) is nearly the same for the p3 and p6 cases and does not vary systematically with the CAPE of the initial sounding. However, because our calculations of PE depend on our selection of 20 min as the lag between

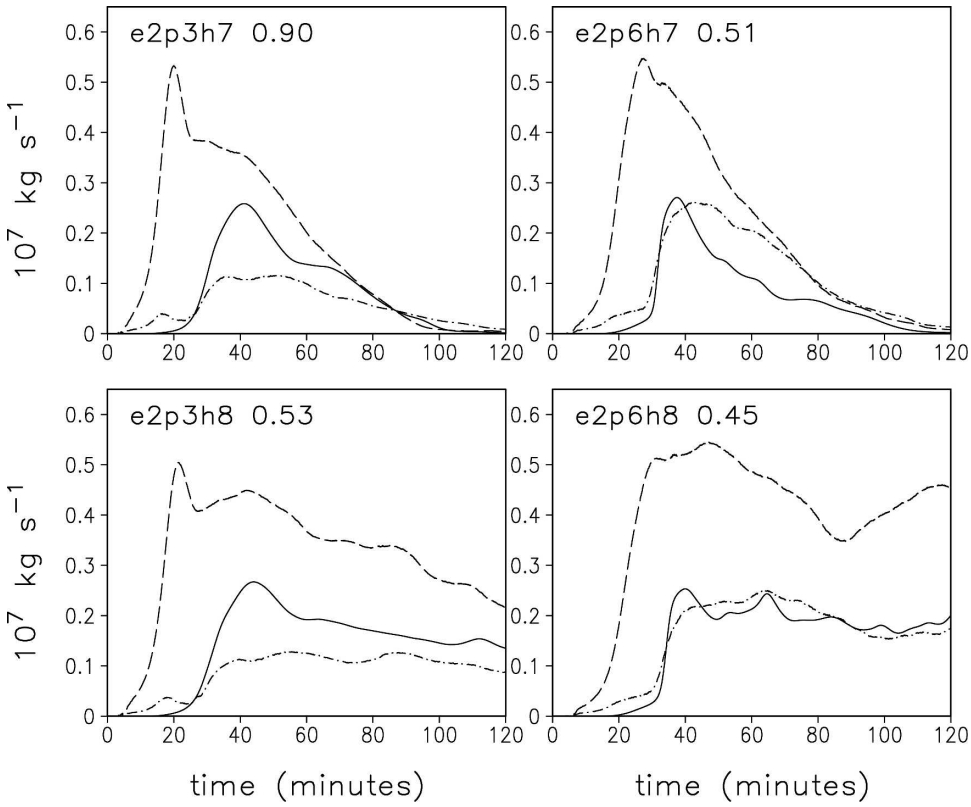

FIG. 6. Same as in Fig. 2 but for the simulations with reduced initial relative humidity.

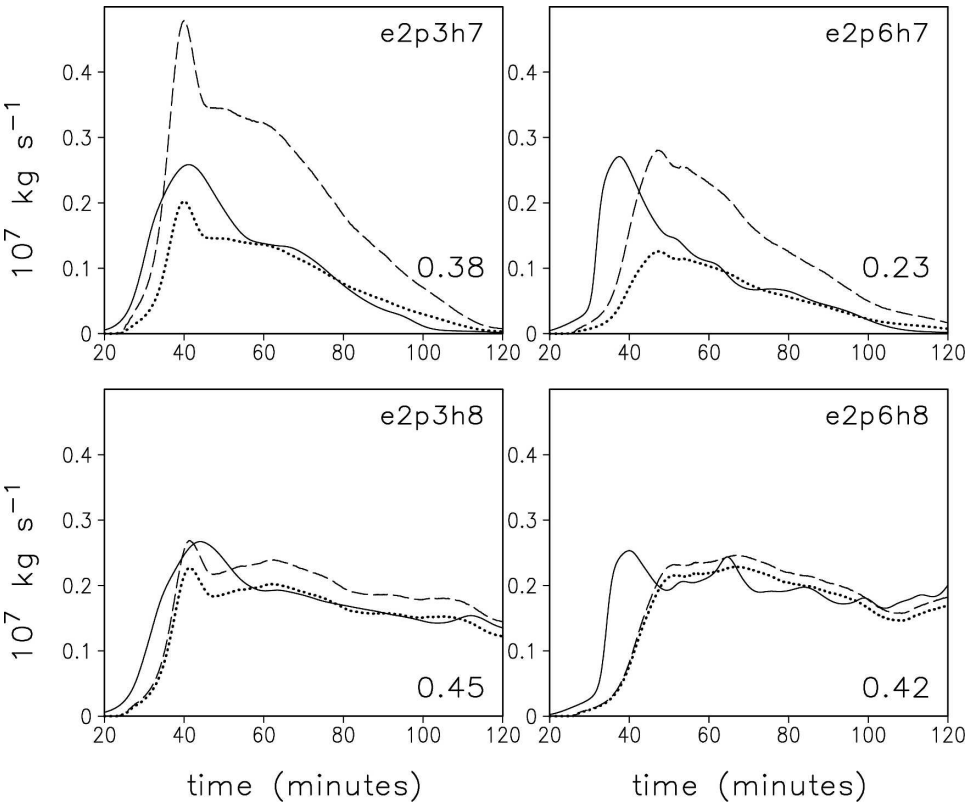

FIG. 7. Same as in Fig. 5 but for the simulations with reduced initial relative humidity.

condensation and precipitation, we must examine this in more detail.

As above, we compute a PE that provides the best fit between the time series of the precipitation rate for 60 to 120 min and the time series of the condensation rate for an earlier period multiplied by the PE. This is done for lags ranging from 0 to 40 min (Fig. 8). (The PE computed here with a lag of zero should not be expected to match the numbers printed in Fig. 6, because the latter were computed from the time-averaged precipitation and condensation rates.) As noted above, for five of the six h9 cases, the PE increases significantly with the lag because the precipitation and condensation rates are both increasing with time. The exception is e1p3h9, for which PE increases only slightly with the lag. For the simulations with lower RH, where the convection is dissipating during the second hour, PE decreases with increasing lag.

Our conclusion that PE does not vary significantly with the environmental precipitable water (p3 versus p6, equivalent to environmental temperature) is seen from Fig. 8 to depend on to only a modest extent the choice of lag for the e2 and e3 cases, as long as the chosen lags are similar for p3 and p6. However, as shown in section 3b, the selection of a 20-min lag is justified. The decrease in PE for a drier environment is independent of the lag for the p6 cases and also for the p3 cases if the lag is more than about 15 min.

All of the precipitation efficiencies examined so far represent averages over time. Figure 9 shows time series of instantaneous PE using a lag of 20 min, for the precipitation reaching the ground during the second hour. Earlier in the simulations, when the storms are beginning to develop, the results are not useful. For the h9 and h8 simulations, the PE varies only moderately over time, with fluctuations of roughly 10%–20% about the long-term mean. Precipitation efficiency changes substantially over time only for the h7 cases, late in the simulations when the storms are dissipating (cf. Fig. 9 with Figs. 6 and 7). In these low FTRH cases, the variations in PE can approach or exceed 50% of the long-term mean.

In observational studies of PE, Fankhauser (1988) noted that water vapor inflow and rainout should ideally be integrated over the lifetime of a storm, but such coverage is seldom available. Similarly, in numerical simulations that do not include the entire lifetimes of the storms, a lag must be estimated. For the present simulations, our conclusions are not highly dependent on the choice of a 20-min lag, and that choice is to some extent justified by the data.

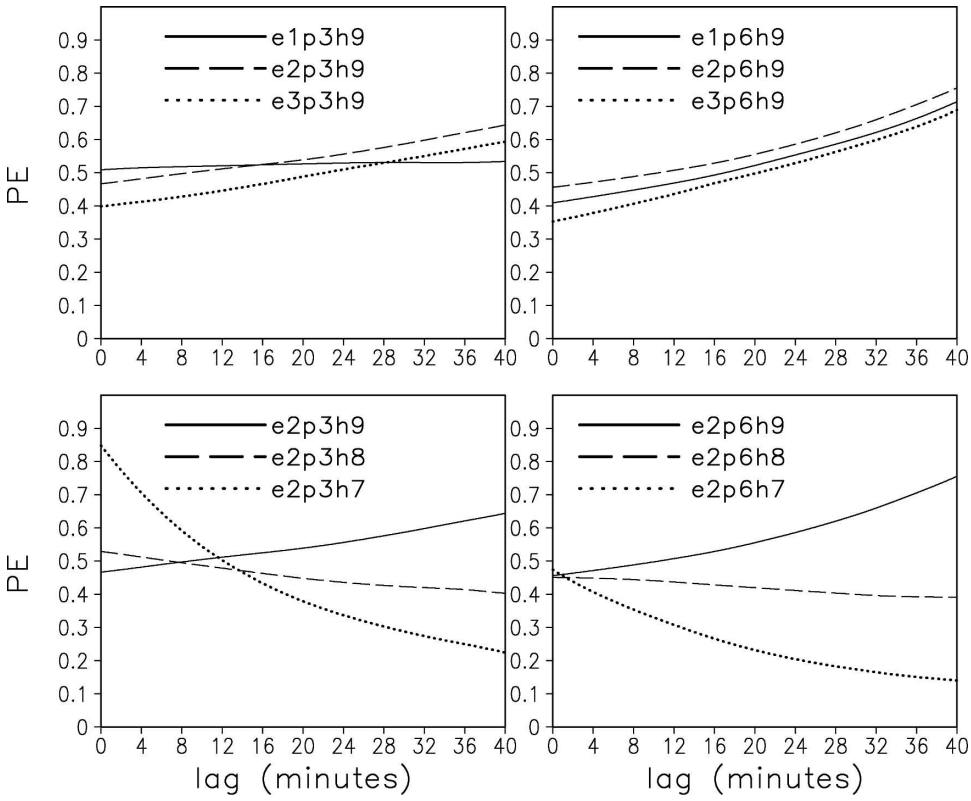

FIG. 8. The precipitation efficiency that provides the best fit between the condensation rate multiplied by the precipitation efficiency and the precipitation rate, as a function of lag.

4. Conclusions

Any discussion of precipitation efficiency must explicitly state how the quantity is defined and be consistent in its definition. McCaul et al. (2005) identified the relatively inefficient conversion of cloud water to precipitation in the p3 simulations and inferred a smaller MPE (defined above in section 1). However, they also showed that there is relatively less evaporation in the p3 simulations, resulting in a smaller ratio of downdraft to updraft mass flux. With the new simulations, we can now see that the combined effect of the decreased production of precipitation and the decreased evaporation is that the temperature of the initial soundings has no significant influence on the MPE.

Similar counteracting effects were described by Cohen and McCaul (2006), who examined the sensitivity of simulated storms to variations in prescribed microphysics parameters. They found that the precipitation rate at the ground is not very sensitive to changes in the value of the shape parameter, ν, in gamma distributions of precipitating hydrometeors or to the specified mean size of the hail and graupel. For example, with the larger value of ν, there is a greater production of precipitation by collection of cloud water but also a larger rate of evaporation of the liquid precipitation.

Lau and Wu (2003) concluded that, in the Tropics, PE of heavy rain associated with deep convection is independent of SST. Superficially, our results appear similar, but they are difficult to compare rigorously, because it is not clear exactly what type of PE they are computing with their proxy data. Rapp et al. (2005) agreed with the conclusion of Lau and Wu (2003), but they admitted that what they computed with their proxy data is not exactly a PE.

Lindzen et al. (2001) proposed, with their adaptive infrared iris hypothesis, that as the SST rises, precipitation efficiency of convective clouds increases, which results in a decrease in the amount of cirrus detrainment. The simulations of McCaul et al. (2005) might seem to support this hypothesis, for which Lindzen et al. (2001) defined PE as the efficiency of conversion of cloud water to precipitation, which is one component of an MPE. The present results related to net boundary fluxes of condensate (Table 1), almost entirely associated with anvil outflow, also appear to lend support to this hypothesis: anvil outflows are always smaller for p6 experiments than for p3 experiments. But perhaps Del

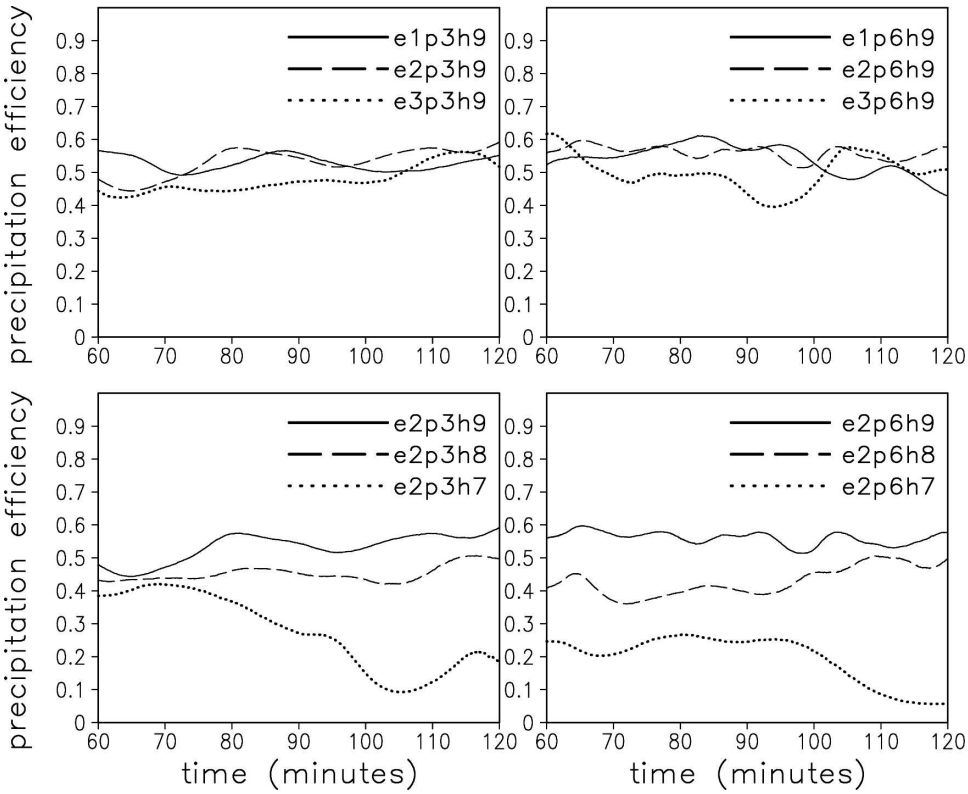

FIG. 9. The instantaneous precipitation efficiency using a lag of 20 min. The times on the horizontal axes apply only to the precipitation; the precipitation is divided by the condensation that occurred 20 min earlier.

Genio et al. (2005) are more correct in using what we have called a CPE to investigate the iris hypothesis. The current results show that when PE is defined as the temporally lagged ratio of precipitation at the ground to condensation plus deposition, PE in simulated convective storms does not change with LCL temperature, all other key parameters being kept constant. It is very difficult, however, to apply our simulation results directly to the adaptive infrared iris hypothesis because we do not know how the real-world precipitation rate would vary, or how the condensation plus deposition rate would vary, as the SST increases. We also do not know how the other key characteristics of the environment, such as wind shear, CAPE, LCL, LFC, and relative humidity, would vary. Using a numerical model to rigorously determine how the large-scale mean cirrus detrainment might change in a warming climate would require much longer simulations than were done here, with a much larger domain and well-validated microphysics.

Stewart et al. (1998) discussed the relevance of the ice crystal growth habit, which depends on temperature, to the production of precipitation. Although growth habit is not a function of temperature in the model we are using, this is not an important limitation in the present simulations of deep convection, in which precipitation is produced mostly by accretion of cloud water by rain, hail, and graupel and by autoconversion. However, we must conclude that our results concerning PE are specific to deep convection.

We have examined the sensitivity of PE to environmental temperature, with other properties of the environment held constant. Our results may therefore not be relevant to comparisons of PE between environments that differ in other properties in addition to temperature, such as cloud condensation nuclei.

Perhaps our most important conclusion is that if storms are not in a steady state, or if the entire life cycles of the storms are not included in the data, the lag between precipitation rates and condensation rates must be considered in the calculation of PE.

Acknowledgments. This research is a part of the Convection Morphology Parameter Space Study (COMPASS), which is supported by Grant ATM-0126408 from the National Science Foundation, under the supervision of Dr. Stephan Nelson. For additional information on the COMPASS study, see our Website at http://space.hsv.usra.edu/COMPASS. The COMPASS

numerical simulations were conducted on the Matrix Linux cluster at the University of Alabama in Huntsville (UAH). We also acknowledge programming support from Jayanthi Srikishen of USRA Huntsville and computer system support from Scott Podgorny, UAH, throughout this project.

REFERENCES

Auer, A. H., Jr., and J. D. Marwitz, 1968: Estimates of air and moisture flux into hailstorms on the High Plains. *J. Appl. Meteor.,* **7,** 196–198.

Brooks, H. E., and R. B. Wilhelmson, 1992: Numerical simulation of a low-precipitation supercell thunderstorm. *Meteor. Atmos. Phys.,* **49,** 3–17.

Browning, K. A., C. W. Pardoe, and F. F. Hill, 1975: The nature of orographic rain at wintertime cold fronts. *Quart. J. Roy. Meteor. Soc.,* **101,** 333–352.

Bryan, G. H., and J. M. Fritsch, 2002: A benchmark simulation for moist nonhydrostatic numerical models. *Mon. Wea. Rev.,* **130,** 2917–2928.

Cohen, C., and E. W. McCaul Jr., 2006: The sensitivity of simulated convective storms to variations in prescribed single-moment microphysics parameters that describe particle distributions, sizes, and numbers. *Mon. Wea. Rev.,* **134,** 2547–2565.

Cooper, H. J., M. Garstang, and J. Simpson, 1982: The diurnal interaction between convective and peninsular-scale forcing over south Florida. *Mon. Wea. Rev.,* **110,** 486–503.

Cotton, W. R., M.-S. Lin, R. L. McAnelly, and C. J. Tremback, 1989: A composite model of mesoscale convective complexes. *Mon. Wea. Rev.,* **117,** 765–783.

Cui, Z., and K. S. Carslaw, 2006: Enhanced vertical transport efficiency of aerosol in convective clouds due to increases in tropospheric aerosol abundance. *J. Geophys. Res.,* **111,** D15212, doi:10.1029/2005JD006781.

Del Genio, A. D., W. Kovari, M.-S. Yao, and J. Jonas, 2005: Cumulus microphysics and climate sensitivity. *J. Climate,* **18,** 2376–2387.

Doswell, C. A., H. E. Brooks, and R. A. Maddox, 1996: Flash flood forecasting: An ingredients-based methodology. *Wea. Forecasting,* **11,** 560–581.

Fankhauser, J. C., 1988: Estimates of thunderstorm precipitation efficiency from field measurements in CCOPE. *Mon. Wea. Rev.,* **116,** 663–684.

Ferrier, B. S., J. Simpson, and W.-K. Tao, 1996: Factors responsible for precipitation efficiencies in midlatitude and tropical squall simulations. *Mon. Wea. Rev.,* **124,** 2100–2125.

Frank, W. M., and C. Cohen, 1987: Simulation of tropical convective systems. Part I: A cumulus parameterization. *J. Atmos. Sci.,* **44,** 3787–3799.

Hudak, D. R., and R. List, 1988: Precipitation development in natural and seeded cumulus clouds in southern Africa. *J. Appl. Meteor.,* **27,** 734–756.

Knight, C. A., and N. C. Knight, 2001: Hailstorms. *Severe Convective Storms, Meteor. Monogr.*, No. 50, Amer. Meteor. Soc., 223–254.

Lau, K. M., and H. T. Wu, 2003: Warm rain processes over tropical oceans and climate implications. *Geophys. Res. Lett.,* **30,** 2290, doi:10.1029/2003GL018567.

Lindzen, R. S., M.-D. Chou, and A. Hou, 2001: Does the earth have an adaptive infrared iris? *Bull. Amer. Meteor. Soc.,* **82,** 417–432.

Lucas, C., E. J. Zipser, and B. S. Ferrier, 2000: Sensitivity of tropical west Pacific oceanic squall lines to tropospheric winds and moisture profiles. *J. Atmos. Sci.,* **57,** 2351–2373.

McCaul, E. W., Jr., and M. L. Weisman, 2001: The sensitivity of simulated supercell structure and intensity to variations in the shapes of environmental buoyancy and shear profiles. *Mon. Wea. Rev.,* **129,** 664–687.

——, and C. Cohen, 2002: The impact on simulated storm structure and intensity of variations in the mixed layer and moist layer depths. *Mon. Wea. Rev.,* **130,** 1722–1748.

——, and ——, 2004: The initiation, longevity, and morphology of simulated convective storms as a function of free-tropospheric relative humidity. Preprints, *22d Conf. on Severe Local Storms,* Hyannis, MA, Amer. Meteor. Soc., CD-ROM, 8A.5.

——, ——, and C. Kirkpatrick, 2005: The sensitivity of simulated storm structure, intensity, and precipitation efficiency to the temperature at the lifted condensation level. *Mon. Wea. Rev.,* **133,** 3015–3037.

Medvigy, D., P. R. Moorcroft, R. Avissar, and R. L. Walko, 2005: Mass conservation and atmospheric dynamics in the Regional Atmospheric Modeling System (RAMS). *Environ. Fluid Mech.,* **5,** 109–134.

Mohamed, Y. A., B. J. J. M. van den Hurk, H. H. G. Savenije, and W. G. M. Bastiaanssen, 2005a: Hydroclimatology of the Nile: Results from a regional climate model. *Hydrol. Earth Syst. Sci.,* **9,** 261–276.

——, ——, ——, and ——, 2005b: Impact of the Sudd wetland on the Nile hydroclimatology. *Water Resour. Res.,* **41,** W08420, doi:10.1029/2004WR003792.

Pielke, R. A., and Coauthors, 1992: A comprehensive meteorological modeling system—RAMS. *Meteor. Atmos. Phys.,* **49,** 69–91.

Raddatz, R. L., 2005: Moisture recycling on the Canadian Prairies for summer droughts and pluvials from 1997 to 2003. *Agric. For. Meteor.,* **131,** 13–26.

Rapp, A. D., C. Kummerow, W. Berg, and B. Griffith, 2005: An evaluation of the proposed mechanism of the adaptive infrared iris hypothesis using TRMM VIRS and PR measurements. *J. Climate,* **18,** 4185–4194.

Rauber, R. M., N. F. Laird, and H. T. Ochs III, 1996: Precipitation efficiency of trade wind clouds over the north central Pacific Ocean. *J. Geophys. Res.,* **101,** 26 247–26 253.

Schär, C., D. Luthi, U. Beyerle, and E. Heise, 1999: The soil–precipitation feedback: A process study with a regional climate model. *J. Climate,* **12,** 722–741.

Shepherd, J. M., B. S. Ferrier, and P. S. Ray, 2001: Rainfall morphology in Florida convergence zones: A numerical study. *Mon. Wea. Rev.,* **129,** 177–197.

Stewart, R. L., K. K. Szeto, R. F. Reinking, S. A. Clough, and S. P. Ballard, 1998: Midlatitude cyclonic cloud systems and their features affecting large scales and climate. *Rev. Geophys.,* **36,** 243–273.

Tripoli, G. J., and W. R. Cotton, 1981: The use of ice-liquid water potential temperature as a thermodynamic variable in deep atmospheric models. *Mon. Wea. Rev.,* **109,** 1094–1102.

——, and ——, 1982: The Colorado State University three-dimensional cloud/mesoscale model—1982. Part I: General theoretical framework and sensitivity experiments. *J. Rech. Atmos.,* **16,** 185–220.

Walko, R. L., W. R. Cotton, M. P. Meyers, and J. Y. Harrington, 1995: New RAMS cloud microphysics parameterization. Part I: The single-moment scheme. *Atmos. Res.,* **38,** 29–62.

Weisman, M. L., and J. B. Klemp, 1982: The dependence of numerically simulated convective storms on vertical wind shear and buoyancy. *Mon. Wea. Rev.,* **110,** 504–520.